$CCIBA^*$: An Improved BA^* Based Collaborative Coverage Path Planning Method for Multiple Unmanned Surface Mapping Vehicles

Yong Ma, *Member, IEEE*, Yujiao Zhao, Zhixiong Li, *Senior Member, IEEE*, Huaxiong Bi, Jing Wang, Reza Malekian, *Senior Member, IEEE*, and Miguel Angel Sotelo, *Fellow, IEEE*

***Abstract*— The main emphasis of this work is placed on the problem of collaborative coverage path planning for unmanned surface mapping vehicles (USMVs). As a result, the collaborative coverage improved BA^* algorithm ($CCIBA^*$) is proposed. In the algorithm, coverage path planning for a single vehicle is achieved by task decomposition and level map updating. Then a multiple USMV collaborative behavior strategy is designed, which is composed of area division, recall and transfer, area exchange and recognizing obstacles. Moverover, multiple USMV collaborative coverage path planning can be achieved. Consequently, a high-efficiency and high-quality coverage path for USMVs can be implemented. Water area simulation results indicate that our $CCIBA^*$ brings about a substantial increase in the performances of path length, number of turning, number of units and coverage rate.**

***Index Terms*— Multiple USMVs, collaborative coverage, path planning, $CCIBA^*$, task decomposition.**

I. Introduction

UNMANNED surface vessels (USVs) are maritime intelligent platforms that can navigate autonomously and safely in various marine environments [1], [2]. Unmanned surface mapping vehicles (USMVs) can improve the efficiency of marine surveying and mapping, while reducing the mapping cost and operational risk of underwater topographic mapping. Consequently, it is intensely suitable for replacing or assisting traditional marine mapping and has broad application prospects [3], [4]. Path planning is one of the key technologies for USMVs to perform tasks [5], [6].

While benefitting from the advantages of wide vision and large coverage of unmanned aerial vehicles (UAVs), UAVs are also widely used in reconnaissance, supervision, water surface search and other fields. However, the USMVs play an irreplaceable role in underwater scanning and long-distance and long-term continuous tasks. Currently, a single USMV is easily restricted by factors, such as endurance and operational efficiency during measurement operations while the multiple USMV collaborative mapping can improve the efficiency of area coverage operations [7], [8] and shorten the time to complete tasks. Therefore, the multiple USMV collaborative mapping has a better task execut ability. As the foundation and prerequisite for the development of marine collaborative mapping operations, it is indispensable to study the multiple USMV collaborative coverage path planning problem [9].

Global coverage path planning has a wide applications in USMVs, such as marine search and rescue, as well as underwater terrain and island and reef surveys. The coverage path planning issue demands to plan paths for USMVs to cover all areas except the obstacles in the target area, keep clear all obstacles, and avoid repeated traversals.

The collaborative coverage improved BA^* algorithm ($CCIBA^*$) is proposed to address the multiple USMV collaborative coverage path planning problem. $CCIBA^*$ is developed based on single vehicle coverage path planning and multiple USMV collaborative behavior. Using the developed $CCIBA^*$ algorithm, the coverage area is divided into several parts according to the number of USMVs. Each USMV can independently plan the coverage path according to the divided subtask area. It is worth noting that through the multiple USMV collaborative behavior strategy, all USMVs are allowed to independently adjust the initially divided sub task area to optimize the whole task time and sailing distance.

Manuscript received 30 January 2021; revised 30 December 2021 and 18 March 2022; accepted 22 April 2022. Date of publication 13 May 2022; date of current version 11 October 2022. This work was supported in part by the National Science Foundation of China under Grant 52022073, Grant 62073251, and Grant 51979261; in part by the Excellent Youth Foundation of Hubei Scientific Committee under Grant 2020CFA055; in part by the Innovation Research Team Project of the Hainan Natural Science Foundation under Grant 722CXTD518; in part by the Research Project of Wuhan University of Technology Chongqing Research Institute under Grant YF2021-12; and in part by the Narodowego Centrum Nauki, Poland, under Grant 2020/37/K/ST8/02748. The Associate Editor for this article was B. B. Gupta. *(Corresponding authors: Zhixiong Li; Yong Ma.)*

Yong Ma, Yujiao Zhao, Huaxiong Bi, and Jing Wang are with the Hubei Key Laboratory of Inland Shipping Technology, School of Navigation, Wuhan University of Technology, Wuhan 430063, China, also with the Sanya Science and Education Innovation Park, Wuhan University of Technology, Sanya 572000, China, and also with the Chongqing Research Institute, Wuhan University of Technology, Chongqing 401120, China (e-mail: myongdl@whut.edu.cn; zhaoyujiaosl@126.com; bihuaxiong96@gmail.com; 1227566341@qq.com).

Zhixiong Li is with the Faculty of Mechanical Engineering, Opole University of Technology, 45758 Opole, Poland, and also with the Yonsei Frontier Laboratory, Yonsei University, Seodaemun-gu, Seoul 03722, Republic of Korea (e-mail: zhixiong.li@ieee.org).

Reza Malekian is with the Department of Computer Science and Media Technology, Malmö University, 20506 Malmö, Sweden (e-mail: reza.malekian@ieee.org).

Miguel Angel Sotelo is with the Department of Computer Engineering, University of Alcalá, 28801 Alcalá de Henares, Spain (e-mail: miguel.sotelo@uah.es).

Digital Object Identifier 10.1109/TITS.2022.3170322

Some highlights of our work are as follows:

(1) In response to the multiple USMVs coverage path planning problem, the $CCIBA^*$ is proposed with the consideration of collaborative requirements, including area division, recall and transfer, area exchange and recognizing obstacles. A collaborative behavior strategy has been designed to achieve efficient collaborative operations of multiple USMVs.

(2) The task decomposition method and level map updating method have been designed in the proposed $CCIBA^*$ algorithm. The path coverage rate and algorithm performances of our $CCIBA^*$ are much better than others. Contrast simulations and real island scenes based simulations are carried out. Moreover, the results are compared to those from *Boustrophedon* and BA^*, which verify the feasibility of our $CCIBA^*$.

II. Related Works

A. Coverage Path Planning for a Single Vehicle

As a result of the above issues in coverage path planning, relevant researchers have carried out quite a few research works. For the implementation of underwater glider mapping in an environment with obstacles, a complete-coverage path-planning obstacle-avoidance algorithm was proposed [10]. The algorithm in [10] ensured that underwater gliders shall be mapped safely against obstacles during their mapping under the premise of ensuring coverage rates. In terms of adjacent path planning, [11] proposed an adaptive multimodal continuous ant colony optimization algorithm for the problem of a multitude of local optima [12]. An algorithm called ε^* was proposed based on the grid method [13] to perform online coverage path planning in unknown environments [14]. The ε^* algorithm was established based on the concept of exploring Turing machines, but it was not affected by local optima. A local path planning method was presented for robots equipped with circular area sensing sensors [15], where triangular decomposition is first performed on the task area and the observation points are then determined to connect them to form a path using the nearest neighbor algorithm. A rainbow coverage path planning method was proposed to perform robot coverage path planning based on sensors in a dynamically changing environment [16]. [17] introduced the concept of foraging and predation risk in predator-prey relationships into their predator-prey coverage path planning algorithm ($PPCPP$). The $PPCPP$ can quickly adapt to unforeseen changes in real-time, and it achieved not only timely and effective responses of unknown changes in a mapping area but also complete coverage of the area with minimal costs. To solve the computationally intractable problem of multiple objectives of coverage path planning, [18] proposed a mixed integer linear programming model. Based on the proposed model, they solved the multiple aircraft coverage path planning problem.

B. Collaborative Coverage Path Planning for Multiple Vehicles

With the increasing application and study of USVs, a single USV cannot complete coverage tasks in complicated operating scenarios. Multiple USMV collaborative mapping has better task execution and fault tolerance capabilities [19]. A deep neural network was applied in the three-dimensional path planning of autonomous robots to embed the decomposition and synthesis of actions [20]. [20] presented a three-dimensional path planning network, where three-dimensional actions were predicted through a two-dimensional convolutional neural network. Therefore, three dimensional path planning has strong real-time performance. For coverage path planning issues based on multirobot dynamic sensors, [21] proposed a method based on solutions to capacitated arc routing issues. The replanning algorithm was used to solve the unknown environmental information. Because of the distributed path planning issues for multiple flying robots, a manually weighted spanning tree coverage algorithm was proposed in [22]. Each robot constructed a spanning tree at the same time to make a good tradeoff between efficiency, redundancy and coverage of the collaborative coverage. A neural dynamics method was proposed to achieve multirobot collaboration and complete coverage path planning [23], where each robot acts as an obstacle to other robots. A group robot coverage path planning model was designed based on the bioinspired neural network to achieve individual dynamic path planning for each robot.

In tasks with large areas, the efficiency could be improved by using multiple USMV collaborative operations. However, there are still many issues to be solved to enable full play to the advantages of multiple USMVs, and collaboration of multiple USMVs should be the most critical [24]–[26]. The quality of task decomposition and collaboration directly affects the efficiency of multiple USMV coverage path planning. There remains space for promotion for the study of multiple USMV collaborative coverage path planning.

III. Problem Formulation

Notations	Definition
G	The map space
g_α	The grid individual space
G_O	The obstacle areas
G_F	The obstacle-expanded forbidden areas
G_C	The navigable waters where USMV needs to perform the depth sounding task
U	The set of USMVs
P	The entire task area
H_i	The task performance index
P_i	The area percentage of the ith subtask area
P_F	The free space
G^m	The list of the global map grids
g_α^m	The individual space of the global map grid
R_{G^m}	The overall task based on G^m
R_i	The subtask numbered i
I	The number of USMVs and subareas
S^m	The list of the global states
O	The start state
Q_{ini}	The initial task assignment
Q_{re}	The collaborative task decomposition
E	The end state
COM	The calculation state
ξ	The recall list

ξ^i	The recall list of ith subarea
CS_{P_i}	The area depth sounding task state of $USMV_i$ in the current subarea
FN	Finished
UFN	Unfinished
tp_m	The grid index value in the global map of the next target point where USMV is located
OC	The task instruction of USMV
OC_m	The task instruction of USMV in the global map, it has the higher priority than OC
tn	To guide USMVs to execute normal coverage tasks in the subarea
te	To guide USMVs to start switching areas and coordinate the coverage tasks between areas
tc	To guide USMVs to start tasks
th	To guide USMVs to continue to cover the new area
tr	To guide USMVs to arrive the unnormal state after local optimum
BL_l^m	The lth-level global map
BL_l^i	The lth-level of the ith subarea
BL_0^m	The most refined grid map
BL_0^i	The 0-level of the ith subarea
G_l^m	The grids list of all levels of global map
G_l^i	The grids list of all levels of the ith subarea
g_α^{ml}	The grid individual space in G_l^m
GT_{list}	The set of grid states
obs	The space for obstacle
exp	The free space for task finished
ue	The free space for task unfinished
fz	The forbidden space
BS	The set of behavior strategies
ex_1	The area division behavior
ex_2	The recall and transfer behavior
ex_3	The area exchange behavior
ex_4	The recognition of obstacle behavior
N_{ml}	The biggest number of grids in G_l^m
L	The highest level of map
$D^0(\omega)$	The detection area of USMV in the grid map under the current position
F^0	The priority area, the grid that satisfies connecting line between itself and ω does not pass through the grids with state fz or obs and its potential energy value is positive
ω	The grid that USMV located in currently
η	The position of obstacle
$BV_{F^l(\omega)}$	The potential energy value of the priority area in current map level
$BV_{\alpha_0}(t)$	The potential energy value of the grid α_0 in BL_0-level map at time t
$BV_{G_0}(0)$	The potential energy value of obstacle grid in BL_0-level map at the initial time
$GT_{\alpha_0}(t)$	The state of the grid α_0 in BL_0-level map at time t

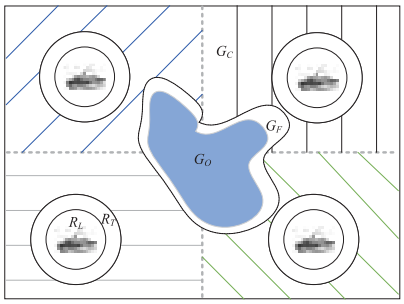

Fig. 1. Schematic diagram of multiple USMV coverage path planning elements.

VAL	The set of potential energy values of all grids in every level map
VAL^l	The set of potential energy values of all grids in l-level map
ω^N, ω^S	The grids at north and south in $D^0(\omega)$
tp_{obs}	The grid in $\{\omega^N, \omega^S\}$ and adjacent to obstacle
$J(tp)$	Potential cost of selected tp

Acronyms	**Descriptions**
$USMV$	Unmanned surface mapping vehicle
$CCIBA*$	The collaborative coverage improved $BA*$ algorithm
$PPCPP$	The predator-prey coverage path planning algorithm

A. Definition

The relevant elements are defined and assumed primarily for the multiple USMV coverage path planning study. As shown in Fig. 1, there are USMVs, grid maps, detection equipment, obstacles and expanded areas in our task execution area.

The initialization of USMVs and grids is defined as follows:

(1) Location information: Our USMV has a positioning device that can obtain its accurate geographic or map relative location and define its current location as μ.

(2) Map updating: Our USMV has detection equipment such as a laser radar that can accurately identify the position of any obstacle in its detection range, and the detection radius is R_L.

(3) Mapping radius: The depth sounding radius of our USMV is R_T.

(4) Grid restriction: All spaces of the map have corresponding grids, and the grid spaces are mutually exclusive as follows:

$$G = \{g_\alpha, \alpha = 1, \ldots, N\} \tag{1}$$

$$g_\alpha \cap g_\beta = \varnothing, \quad \forall g_\alpha,\ g_\beta \in G \wedge \alpha \neq \beta \tag{2}$$

where G is the map space, α and β are grid serial numbers, N is the maximum grid series in the map, and g_α and g_β are grid individual spaces. To ensure accurate coverage, the areas g_α and g_β are slightly larger than the envelope area occupied by our USMV and within the R_L of our USMV.

(5) Grid properties: As shown in Fig. 2, the grids in G can be divided into three categories G_O, G_F and G_C. G_O, G_F and G_C represent the obstacle, the obstacle-expanded no-sail areas and the navigable waters where our USMV needs to perform the depth sounding task, respectively.
(6) Completed coverage: While the depth sounding equipment of our USMV completes the depth sounding tasks in all areas G_C, the traversal depth sounding task ends.

B. Subarea Division Based on Task Performance

A subarea division method [27] is proposed by combining the task performances of our USMV.

(1) Multiple USMVs: A set of multiple USMVs $U = \{USMV_i | 1 \le i \le I\}$ is established. The core goal of collaborative coverage can be regarded as designing an algorithm to enable i USMVs to fully traverse the entire task area P under the premise of their full efficiencies.
(2) Task performances: In accordance with performances or the ability to perform coverage tasks of the $USMV_i$, a task performance index $H_i, i = 1, \ldots, I$ is proposed, whose size depends on the performances of USMV sensors, task functions, energy consumption limits and other factors, and $\sum_{i=1}^{I} H_i = 1$ exists.
(3) Area division: The area is divided into I parts in light of the number of USMVs, each of which is expressed as its area percentage as follows: ($P_i, i = 1, \ldots, I$, $0 < P_i < 1$ and $\sum_{i=1}^{I} P_i = 1$).
(4) Grid restriction: Each grid α in the free space P_F of P has been scanned at least by any $USMV_i$ as follows.

$$Y(\alpha, i) = \begin{cases} 1, & BV_{\alpha}^{i}(t) \le 0 \\ 0, & else \end{cases} \tag{3}$$

$$\sum_{USMV_i \in U} Y(\alpha, i) \ge 1, \quad \forall \alpha \in P_F \tag{4}$$

(5) Planning goal: For multiple USMVs collaborative coverage, the following factors are primarily considered: the overall coverage path, time and rate, and the single coverage performances, which can be seen in the equation as follows:

$$\min \varphi = k_1 \cdot \sum_{i=1}^{I} P_i(d_{cost}) + k_2 \cdot \max_i P_i(t_{cost}) \tag{5}$$

$$S.T. \begin{cases} \sum_{i=1}^{I} P_i = 1 \\ k_1 + k_2 = 1 \\ \sum_{USMV_i \in U} Y(\alpha, i) \ge 1, \forall \alpha \in P_F \end{cases} \tag{6}$$

where ϕ is the multiple USMV coverage overall cost model, k_1 is the coverage path cost coefficient, k_2 is the coverage time cost coefficient, $P_i(d_{cost})$ is the estimated coverage path of P_i, and $P_i(t_{cost})$ is the estimated coverage time of P_i.

The segmentation process is shown in Fig. 2. Above all, d_{cost} and t_{cost} of the initial task area are estimated in light of H_i of the $USMV_i$. d_{cost} is further modified in light of the distribution of obstacles Obs, and t_{cost} is adjusted considering the equipment Equ of our USMV. Finally, the reallocated subareas are output.

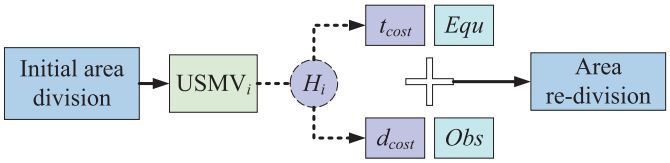

Fig. 2. Subarea division.

C. Typical Collaborative Behavior Strategies

To improve the optimal decision-making level in complex scenarios, four typical collaborative behavior strategies called area division, recall and transfer, area exchange and recognizing obstacles are established for the $CCIBA^*$ algorithm.

Remark 1: Each USMV equips with positioning equipment, the scanning progress and trajectories of USMVs can be obtained in real-time. With the scanning progress and trajectories information of all USMVs, a schedule center would perform a coordinator to command USMVs to adjust task area to reduce the backtracking paths of USMVs and optimize the total voyage.

As shown in Fig. 3, dotted lines, irregular figures and dotted lines represent the area division boundaries, obstacles and area exchange or redistribution involved in collaborative behavior strategies, respectively. As shown in Fig. 3(a), area division scenes involve the temporary allocation of small areas and updating of submaps. For P_2, a small area A_{rea} is formed by obstacles and its area boundary while USMV enters. However, the cost of bypassing obstacles increases due to the effects of the long and narrow terrain while the USMV enters this area. Meanwhile, the USMV may fall into a local optimum in this area, which increases the calculation cost. Therefore, if the USMV in P_1 initially recognizes the edge of an obstacle, this strategy incorporates A_{rea} into P_1 to ensure that the USMV executes coverage tasks in A_{rea} at its convenience while the continuous coverage actions can be guaranteed.

As shown in Fig. 3(b), recall and transfer scenes involve the recall area due to the trend change in the path directions. Multiple USMVs collaborative planning is subject to the independent coverage updating processes of each subarea so that a potential recall area will occur. In this scenario, the $USMV_1$ in P_1 may bypass obstacles shortly after its starting position until the $USMV_1$ has been out of the lower left bound of this area or falls into the local optimum since then. A_{rea} remains a state of unexplored coverage. This strategy divides A_{rea} into P_2 to ensure that the $USMV_2$ in this area can continue entry of A_{rea} to perform additional coverage operations. For P_1, the $USMV_1$ is out of bounds to continuously execute tasks and decompose the tasks in the next area, regardless of its falling into the local optimum.

As shown in Fig. 3(c), area exchange scenes involve the exchange allocation of a larger area. In addition, the area division scenes are differentiated. Due to the effects of obstacles and boundaries, a larger area is divided by P_2, and the

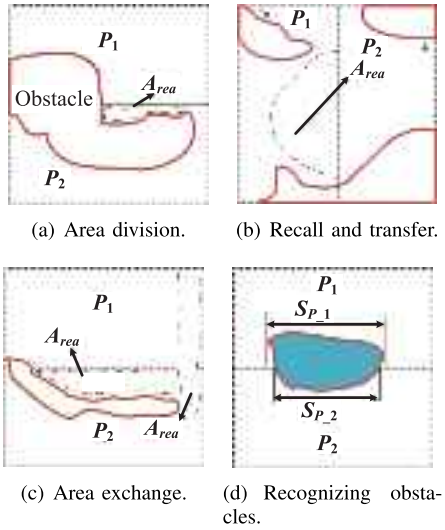

(a) Area division. (b) Recall and transfer. (c) Area exchange. (d) Recognizing obstacles.

Fig. 3. Typical behavior strategies.

continuous performance of tasks in A_{rea_2} increases the path and calculation costs of the $USMV_2$ in P_2. Meanwhile, A_{rea_2} is located in the direction of the primary coverage path of P_1, and A_{rea_1} is located in the direction of the primary coverage path of P_2. Therefore, the strategy can divide A_{rea_1} and A_{rea_2} into P_1 and P_2. In this case, the coverage time and task loads are basically unchanged. Based on the roughly same obstacle bypass costs, there is a slight impact on path lengths.

As shown in Fig. 3(d), scenes for recognizing obstacles are primarily for obstacle processing. In this case, P_1 and P_2 do not involve any redistribution issue, and the USMV is covered normally. Due to updating maps of independent subareas, the paths of bypassing obstacles in individual S_{P_1} and S_{P_1} segments are incomplete for each USMV to determine whether obstacles may be left out. Therefore, map updates of the whole water area may be affected and there could be potential dangers. The process of collaborative recognizing obstacles is also added while the coverage tasks are executed.

IV. Collaborative Coverage Path Planning Algorithm for Multiple USMVs

A. Coverage Path Planning Task Decomposition

Task decomposition is an important issue in the multiple USMV coverage path planning besides task area decomposition. The grid task decomposition is defined as follows:

$$G^m = \{g_\alpha^m, \alpha = 1, \ldots, N\} \tag{7}$$

$$g_\alpha^m \cap g_\beta^m = \varnothing, \quad \forall g_\alpha^m, g_\beta^m \in G^m \wedge \alpha \neq \beta \tag{8}$$

$$R_{G^m} = \bigcup_{i=1}^{I} R_i \tag{9}$$

where G^m is the list of the global map grids, g_α^m and g_β^m are individual spaces of the global map grids,m is the index of sub-task area, N is the maximum number of grids, R_{G^m} is the overall task based on G^m, R_i is the subtask numbered i, and I is the upper bound of the number of task P_i, which corresponds to the number of USMVs participating in the task.

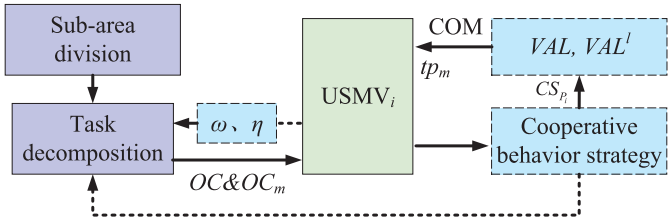

Fig. 4. Task decomposition of $USMV_i$.

During multiple USMV mapping, the global and local states of tasks and map scenes are first distinguished. Based on the integration of all local states, the process of determining the global states and task distribution is added. The primary function is to achieve circulation of the information between various USMVs, collaborative organization and normal operation of the entire algorithm.

The details are as follows:

(1) The definition of states is the state of multiple USMV coverage path planning $S^m = \{O, Q_{ini}, Q_{re}, E, COM\}$, which reflects the overall task flow and internal adjustments. S^m is the list of global states, O is the start state, Q_{ini} is the initial task assignment, Q_{re} is the collaborative task decomposition, E is the end state, and COM is the calculation state.

(2) The backtracking list is defined as $\xi = \{\xi^i, i = 1, 2, \ldots, I\}$. ξ is the recall list, and ξ^i is the recall list of sub-area i.

(3) The subarea information is defined as $CS_{P_i} \in \{FN_i, UFN_i\}$. CS_{P_i} is the area depth sounding task state of the $USMV_i$ in the current subarea, and FN and UFN stand for $Finished$ and $Unfinished$, respectively.

(4) The control instructions of the USMV are defined as $tp_m \in \{1, \ldots, N^m\}$ and $OC_m \in \{tn, te, th\}$. tp_m is the grid index value in the global map of the next target point where USMV is located. For the multiple USMV coverage path planning, tp_m is used to achieve cross-area coordination capabilities. OC_m represents the task instructions of the USMVs in the global map, which have higher authority and priority than subareas. tn is used to guide the USMVs to execute normal coverage tasks in the subarea. te is used to guide USMVs to start switching areas and coordinate the coverage tasks between areas. The th is used to guide the USMVs to continue to cover a new area.

As shown in Fig. 4, the task area is roughly divided and the task is decomposed according to task performances. The $USMV_i$ continuously records and feeds back ω and η and generates obstacle information in real-time. When matching collaborative behaviors, the system is switched to state Q_{re} to redistribute sub-areas if the redistribution requirements are satisfied. tp_m is generated by means of the coverage path planning algorithm to go out of the original area. While it arrives at the designated starting point, it is guided to turn on state th. The $USMV_i$ records the state value CS of its experienced grid and the state value CS_{P_i} of P_i in its operation areas.

B. Map Updating

A map update method including global map update and subarea map update is proposed to ensure the performance of the algorithm. The global map has higher priority and authority and can be intervened when necessary. The subarea map updating processes are in independent states. Each USMV works and updates the global map BL_l^m and the submap BL_l^i. After allocating areas and tasks in P_i and R_i, each BL_l^i is independently updated to complete the multiple USMV coverage task. BL_l^m is primarily applied for collaborative behaviors among the $USMV_i$ between areas to ensure that the $USMV_i$ can have a more favorable choice while its target point is determined by updating its map level in subintervals. Therefore, the overall coverage time can be saved, and the negative effects of states tr and te on the path length can be reduced.

1) Initialization Modeling: The most refined grid map level BL_0^m is established in the global map. Subsequently, the map level BL_0^i of each subarea is established based on BL_0^m. Its specific inclusion area is determined by the initial division of the overall area P. Based on establishment of BL_0^m and BL_0^i, the upgrading instructions are continuously executed as follows:

$$G_l^m = \{g_\alpha^{ml}, \alpha^{ml} = 1, \ldots, N_{ml}\}, \quad \forall ml \in \{0, \ldots, mL\} \tag{10}$$

$$G_l^m = \bigcup_{i=1}^{I} G_l^i \tag{11}$$

where G_l^m is the grid list of all levels of the global map, g_α^{ml} is the grid individual space in G_l^m, and N_{ml} is the maximum number of grids in G_l^m.

Remark 2: To ensure scanning efficiency and area coverage, the task area has been divided into fine grids. The area g_α is slightly larger than the envelope area occupied by USMV and within R_L of USMV, R_L is detection radius of USMV. USMV scale and scanning radius can be used as a standard to divide the grid.

2) BL_0^m-Level Map Modeling and Assignment: The BL_0^m-level map is initialized. After the initial assignment of the BL_0^m-level map, assignment of each BL_0^i map continues, whose potential energy distribution independently starts from each interval P_i. Thus, each grid g_α^{ml} has two potential energy values. However, this process does not considerably increase the amount of calculation. They have a direct and simple conversion relationship; however, BL_0^m may not be active most of the time, similarly to the 0-level map of each interval P_i, but it only occurs in the area collaborative transfer process of the $USMV_i$.

For unknown obstacles, the $USMV_i$ updates $GT\_list = \{obs, exp, fz, ue\}$ in an independent interval P_i. If it is at the boundary of the subarea, the recognition is incomplete. At this time, the $Bresenham$ algorithm is first utilized to rasterize the edges of the identified obstacles into pixels in the frame buffer. The $FloodFill$ algorithm is then introduced to process the recognition results based on the primary principle which is described as follows: a number of connected points are extracted in a closed area and separated from other adjacent areas. After updating obstacles of BL_0^m, the information is passed to each BL_0^i-level map.

C. CCIBA Algorithm*

On the basis of subarea division, and typical behavior strategies, our multiple USMV collaborative coverage path planning algorithm $CCIBA^*$ is proposed in Algorithm 1.

Algorithm 1 $CCIBA^*$ Algorithm

Require:
ω, η, P_i, $BV_{F^l(\omega)}$, VAL
Ensure:
tp, OC, OC_m
1: Initialize $BL_l^i = BL_0^i$, $BL_l^m = BL_0^m$, ω, VAL, P_i and S^m.
2: Input the static environment of $USMV_i$ and set the parameters, including GT_list and $BV_{G_0}(0)$.
3: **if** $BL_l^m = BL_0^m$ **then**
4: **if** $BV_\omega > 0$ **then**
5: **if** $\{\omega^N, \omega^S\} \subset F^0$ **then**
6: $tp = \arg\min J(tp_{obs})$.
7: **else**
8: $tp = \omega$, and set $OC = tc$, $OC_m = tn$.
9: **end if**
10: **if** $F^0 \neq \varnothing$ **then**
11: $tp = \arg\max BV_{F^0(\omega)}$, and set $OC = tc$, $OC_m = tn$.
12: **else**
13: **while** There is no satisfied behavior in BS **do**
14: **if** $F^l \neq \varnothing, 1 \leq l \leq L$ **then**
15: update BL_l^i, and set $OC = tr$.
16: $tp = \arg\max BV_{F^l(\omega)}$.
17: **end if**
18: **end while**
19: **end if**
20: **end if**
21: **end if**

At O stage, the static map is imported and the grid state is initialized. The submap and global map are established synchronously. The $USMV_i$ in subarea P_i outputs its own position information ω and obstacle information η, which are passed to BL_l^i to update BL_l^m.

At BL_0^m-level map stage and BL_l^m-level map stage, in case of $BV_\omega > 0$ and $\{\omega^N, \omega^S\} \subset F^0$, the USMV is put into an independent operation. The potential cost $J(tp)$ is calculated to select the relatively optimal path. Similarly, the orientation is preferentially selected if any side of μ^N and μ^S is adjacent to an obstacle. Obstacles in each interval P_i can be bypassed through this action and processing ex_4 starts at the same time. In case of $BV_\omega > 0$ and while state ue only occurs on one side of μ^N and μ^S and their other side is forbidden, command tc starts to guide the $USMV_i$ to start its coverage task. Moreover, BL_l^i and BL_l^m are updated. In case of $BV_\omega = 0$, $F^0 \neq \varnothing$, $USMV_i$ starts to turn round traversing in the next stage, where the largest value α_0 of BV_{α_0} in F^0 is taken as point tp. If it is determined that the above situations are not met, then the $USMV_i$ is determined to be in a local optimum at this time. Prior to updating the map level, BS is determined. If the collaborative strategy is satisfied, the preset actions start to output command te instruction and update the map for redistribution of P_i. If all situation of BS are not satisfied, the higher BL-level map stage starts to find the path and output command tr.

At E-stage, due to $CS_{P_i} \in \{FN_i, UFN_i\}$, it is determined that coverage tasks of the entire area P ends while $USMV_i$ transmit back FN_i in each area P_i. Those missing areas are reviewed through all detected environmental information to generate the coverage information.

$$BS \in \{ex_1, ex_2, ex_3, ex_4\} \tag{12}$$

where: ex_1, ex_2, ex_3 and ex_4 correspond to the four situations called area division, recall and transfer, area exchange and recognizing obstacles of the collaborative behavior strategies, respectively.

D. Time Complexity Analysis

The analysis of the time complexity of $CCIBA^*$ is carried out on 0-level and high-level maps. The following assumptions are made: there are I USMVs ($USMV_i, i = 1, 2, \ldots, I$) to execute tasks, the submap detection area $D^0(\omega)$ of $USMV_i$ contains N_{i0} grids of 0-level, $D^l(\omega)$ includes N_{il} grids of high-levels, and the detection area of the global map contains N_{m0} grids.

The time complexity of our algorithm is $O(I \times N_{i0})$ in the 0-level map. If I USMVs execute the collaborative strategy, the complexity is $O(I \times N_{i0} + I \times N_{m0})$. While all USMVs performs path planning at the L-level in the worst case and execute the collaborative strategy, the complexity is $O(I \times N_{i0} + I \times N_{m0} + I \times L \times N_{il})$. Thus, the complexity can be regarded as $O(I \times N_{i0} + I \times N_{m0} + I \times L \times N_{il})$.

V. Simulations and Experiment

A. Simulation Analysis of Collaborative Coverage Path Planning

In reference to the simulation of collaborative coverage path planning of USMVs, some works [28], [29] provide useful inspiration in the USMV communication, information perception, image processing and, etc. The dimensionless quantity of the map specification is 200×200, the mapping line width is 5, number of USMVs for performance of the collaborative coverage mapping task is 4 ($USMV_1$, $USMV_2$, $USMV_3$, $USMV_4$). The preset performance indices of USMVs are preset as $H_1 = 0.25$, $H_2 = 0.30$, $H_3 = 0.25$ and $H_4 = 0.20$.

1) Analysis of BA^* Coverage Path: As for simulation of BA^*, the task area is firstly divided. As shown in Fig. 5(a,) the task area is first divided into quarters, and then four USMVs are released to map the areas. The four USMVs are initially berthed off in the shores of their areas. Their starting directions are from their shores to the task waters. It is worth noting that the four USMVs begin to traverse together.

As shown in Fig. 5(b), $USMV_1$ leaves the first critical point on the top of P_1 and consecutively goes in for recall 3 times to finally arrive at the end point. When $USMV_2$ arrives at the critical point on the top of P_2, BA^* maintains that there is no feasible path. Consequently, $USMV_2$ ends the task while an area is missed. $USMV_3$ ends the task while it is backtracked 2 times. $USMV_4$ completes the coverage task in the first unit in area P_4. Table I presents the details of BA^*, *Boustrophedon* and $CCIBA^*$. The analysis shows that BA^* algorithm brings about a low coverage rate in this scenario primarily as $USMV_2$ untimely end of the coverage task.

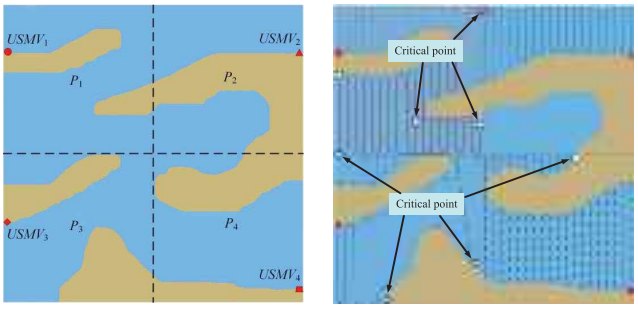

(a) Task area division. (b) The coverage path.

Fig. 5. Coverage paths of BA^* algorithm.

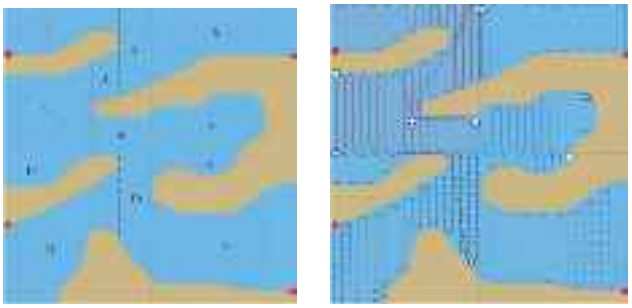

(a) Offline area division. (b) The coverage path.

Fig. 6. Coverage paths of *Boustrophedon* algorithm.

2) Analysis of Boustrophedon Coverage Path: *Boustrophedon* algorithm takes the same initialization processes as BA^* algorithm. Moreover, there are 12 offline decomposition units for the *Boustrophedon* algorithm which is shown in Fig. 6(a). Areas P_1, P_2, P_3 and P_4 contain units 1-5, 6-7, 10-12, and 8-9, respectively.

The complete paths are shown in Fig. 6(b), the coverage paths of *Boustrophedon* are basically consistent with BA^* except P_2, and the fact that the BA^* algorithm brings about missing areas has been avoided in *Boustrophedon*. This results from the *Boustrophedon* algorithm serving as the offline algorithm and the sequences for execution of unit tasks are set in advance. The details of *Boustrophedon* performance are shown in Table I.

3) Analysis of PPCPP in [17] Coverage Path: In this case, the smoothness reward and the boundary reward of the $PPCPP$ algorithm are weighted with $\omega^s = 0.53$ and $\omega^b = 0.48$ according to Case Study 1 of [17].

As shown in Fig. 7, $USMV_1$ repeats some path in the P_1 area, which increases the length of the coverage path. According to the classic cooperative behavior strategy, one part of the P_3 area is separated to P_1. $USMV_2$ continues to cover its remaining task area of P_3 and a part of P_4 after bypassing the obstacle. $USMV_3$ and $USMV_4$ successfully complete their coverage tasks. The details of $PPCPP$ performance are shown in Table I.

4) Analysis of $CCIBA^*$ Coverage Path: As shown in Fig. 8(a), $USMV_1$ goes in for normal traversal after it

Fig. 7. Coverage paths of $PPCPP$ algorithm.

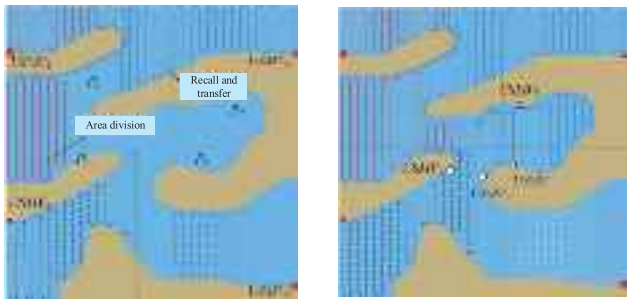

(a) Collaborative behavior strategies. (b) The coverage path.

Fig. 8. Coverage paths of $CCIBA^*$ algorithm.

has bypassed obstacles. Other USMVs continue their normal coverages. In the light of the typical collaborative behavior strategy, a part of P_3 is segmented into P_1. In the subsequent traversing process, a part of the area is exchanged because the segmented area is relatively large. $USMV_1$ finally assumes some tasks in P_3. A part of the area is segmented and exchanged to P_3 in the later stage. After $USMV_2$ traverses out of P_2, its recall and transfer starts to undertake a wide range of areas left out after $USMV_1$ bypasses obstacles.

As shown in Fig. 8(b), $USMV_2$ gradually arrives at the second half of P_2 during its collaborative process and starts bypassing to complete its area coverage task. $USMV_3$ continues its normal coverage. Because $USMV_1$ shares more tasks, some tasks in P_1 are undertaken in light of the area exchange strategy. The segmentation strategies for P_3 and P_4 are also triggered during the coverage process to cover some tasks of $USMV_4$ at its convenience. The performance of $USMV_4$ is poor, and its shared task area is relatively simple. With the cooperation of $USMV_3$ and $USMV_2$, the coverage task in P_4 is finally complete. To verify the performance of our algorithm, the final coverage of our $CCIBA^*$ algorithm is tested. The results are shown in Table I.

5) Comparison and Analysis of Algorithm Performance: Based on the summary of our simulations, a comparative analysis in Table I is performed for the performances of the four algorithms, which include items, such as algorithm type, path length, number of turning, coverage rate, sub-path standard deviation and number of units.

As shown in Table I, comparisons are performed on the path lengths, turnings, units and coverage rates of those four algorithms. The path length and tunings of BA^* stand out since there is a missed area. The path length of our $CCIBA^*$ slightly increases by approximately 0.9% compared with that of the BA^* algorithm, decreases by 10.76% compared with that of the *Boustrophedon* algorithm and decreases by 0.78% compared with that of the $PPCPP$ algorithm.

The number of turning of our $CCIBA^*$ decreases by 5.1% compared with that of BA^* algorithm, 16.5% compared with that of the *Boustrophedon* algorithm and 5.9% compared with that of $PPCPP$ algorithm. Our simulation results indicate that the collaborative allocation and obstacle handling strategies of our $CCIBA^*$ algorithm ensure that its number of turning is greatly reduced.

The number of units for our $CCIBA^*$ algorithm and the $PPCPP$ algorithm falls by 44.4% and 58.3% compared to those of the BA^* and *Boustrophedon* algorithms, respectively. The analysis of their simulation paths indicates that the *Boustrophedon* algorithm as an offline algorithm refines its decomposed units to ensure its coverage rate while the BA^* algorithm decomposes units in real-time due to the demand, and reduces its number of units accordingly. However, our $CCIBA^*$ algorithm greatly weakens the recalls of the collaborative strategy and tries to avoid its optimal layout to ensure that its number of units remains low.

A comparison of coverage rates for the four algorithms is shown in Table I. Analysis of their coverage processes indicates that a large area is missed in P_2 for the BA^* algorithm while a small area is left out for mapping for the *Boustrophedon* algorithm in case of its crossing over units. However, our $CCIBA^*$ algorithm and $PPCPP$ basically maintain complete coverage.

A comparative analysis of path length distributions for the four algorithms is shown in Table I. *Boustrophedon* algorithm strictly enforces the rules of the equal division of areas. Due to the relatively uniform distribution of obstacles, the path lengths of $USMV_1$, $USMV_3$ and $USMV_4$ from *Boustrophedon* are basically the same as those of BA^*. However, the path length of $USMV_2$ is lower for the BA^* algorithm due to its missing mapping. The path length of $USMV_4$ is lower for the $PPCPP$ algorithm because $USMV_2$ favors $USMV_4$. Our $CCIBA^*$ algorithm performs offline planning based on the performances of USMVs, $USMV_1$ and $USMV_3$ have the similar performances with a difference of approximately 137.09 in their path lengths. The path length of $USMV_2$ with strong performance is 773.81 longer than that of $USMV_4$ with weak performance. The collaborative area allocation finally produces the positive effect of a small path length and fewer turning times.

In summary, our simulations indicates that our $CCIBA^*$ algorithm rather than *Boustrophedon*, BA^* and $PPCPP$ algorithms, make considerable improvements in aspects, such as path length, number of turning, number of units and coverage rate.

B. Reef Scene Based Multiple USMVs Collaborative Mapping

As shown in Fig. 9, multiple USMV collaborative mapping is performed on waters near Hengliang Mountain of

TABLE I

PERFORMANCE ANALYSIS TABLE OF BA^*, *Boustrophedon*, $PPCPP$ AND $CCIBA^*$

Algorithm	USMV	Performance H_i	Path length	Percentage	Turning	Coverage rate	Units
BA^*	$USMV_1$	0.25	1674.07	33.19%	42	98.1%	4
	$USMV_2$	0.30	740.74	14.69%	18	60.9%	1
	$USMV_3$	0.25	1220.74	24.20%	28	96.8%	3
	$USMV_4$	0.20	1408.15	27.92%	29	98.3%	1
	Summation	-	**5043.70**	-	**117**	**90.8%**	**9**
Boustrophedon	$USMV_1$	0.25	1674.07	29.35%	42	98.1%	5
	$USMV_2$	0.30	1401.48	24.57%	34	94.9%	2
	$USMV_3$	0.25	1220.74	21.40%	28	96.8%	3
	$USMV_4$	0.20	1408.15	24.68%	29	98.3%	2
	Summation	-	**5704.44**	-	**133**	**95.7%**	**12**
$PPCPP$	$USMV_1$	0.25	1607.77	31.30%	36	96.1%	1
	$USMV_2$	0.30	1491.58	29.03%	32	94.9%	2
	$USMV_3$	0.25	1150.74	22.40%	36	98.3%	1
	$USMV_4$	0.20	886.47	17.27%	17	98.8%	1
	Summation	-	**5136.56**	-	**118**	**97.0%**	**5**
$CCIBA^*$	$USMV_1$	0.25	1348.14	26.48%	32	98.4%	1
	$USMV_2$	0.30	1652.59	32.47%	39	97.9%	2
	$USMV_3$	0.25	1211.05	23.79%	22	97.5%	1
	$USMV_4$	0.20	878.78	17.26%	18	97.3%	1
	Summation	-	**5090.56**	-	**111**	**97.7%**	**5**

TABLE II

PERFORMANCE ANALYSIS TABLE OF COVERAGE PATH PLANNING OF THE WATERS NEAR HENGLIANG MOUNTAIN

USMV	Performance H_i	Path length	Percentage	Turning	Coverage rate	Units
$USMV_1$	0.25	6502.7	21.47%	27	96.5%	1
$USMV_2$	0.25	6576.2	21.71%	24	96.4%	2
$USMV_3$	0.20	7752.0	25.59%	23	97.1%	1
$USMV_4$	0.30	9462.9	31.27%	28	96.7%	1
Summation	-	30293.8	-	102	96.8%	5

the Zhoushan Islands. The mapping line width is set as 25m. $USMV_1$, $USMV_2$, $USMV_3$ and $USMV_4$ collaboratively execute the task. Their performance indices are preset as $H_1 = 0.25$, $H_2 = 0.25$, $H_3 = 0.20$ and $H_4 = 0.30$.

$CCIBA^*$ coverage path planning is shown in Fig. 9 for waters near Hengliang Mountain. Fig. 9(a) shows their collaborative coverage path planning results. Fig. 9(b) schematically illustrates the distribution of traverse lines in the island map.

As shown in Fig. 9(a), $USMV_1$ encounters a whole island in the coverage area, and then it completely bypasses the island and continues to coverage mapping. Meanwhile, $USMV_2$ executes three reciprocating coverages and achieves a local optimum. To overcome the local optimum, map updating is performed. $USMV_3$ begins to bypass obstacles shortly after it begins the task. Subsequently, it bypasses obstacles again after completing four normal reciprocating coverages. It finally complete its coverage and goes ashore. The water area where $USMV_4$ executes its tasks is roughly divided into upper and lower parts due to the distribution of islands. Then, $USMV_4$ finishes the task without falling into the local optimum.

The final coverage of waters near Hengliang Mountain is tested. The results are shown in Table II. According to the final calculation, $USMV_1$, $USMV_2$, $USMV_3$ and $USMV_4$ account for approximately 21.47%, 21.71%, 25.59% and 31.27% of the total path in this task, respectively. Such results basically correspond to their task performances. The final path coverage rate is 96.8%. Therefore, the coverage requirements of multiple USMV collaborative path planning can be satisfied.

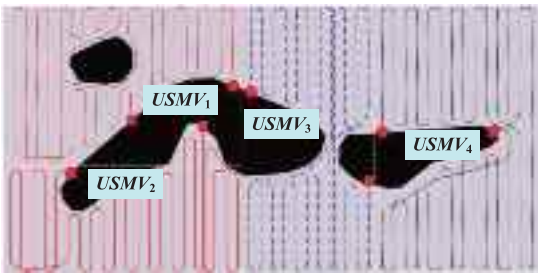

(a) Path planning result.

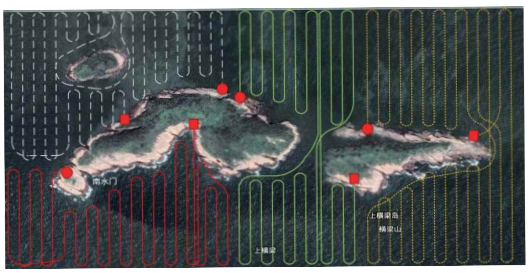

(b) Mapping lines.

Fig. 9. Task area division of waters near Hengliang Mountain.

VI. CONCLUSION

To improve the efficiency of USMV collaborative path planning, the $CCIBA^*$ algorithm is proposed. In the algorithm, the task execution capability differences of USMVs, area division, recall and transfer, area exchange and recognizing obstacles

are fully considered for designing the offline map division method and collaborative behavior strategies. Then, our *CCIBA** algorithm achieves multiple USMV collaborative coverage path planning with a high coverage rate and general algorithm complexity. Simulation analyses are performed to evaluate the performances of *CCIBA**, *Boustrophedon* and *BA** algorithms for multiple USMV coverage path planning. The results indicate that our *CCIBA** algorithm has preferable indices, such as number of turning, coverage rate, number of units and path length. In the near future, our *CCIBA** will be applied to larger-scale surveying and mapping ships, and far-sea mapping survey experiments will be carried out.

REFERENCES

[1] Y. Ma, M. Hu, and X. Yan, "Multi-objective path planning for unmanned surface vehicle with currents effects," *ISA Trans.*, vol. 75, pp. 137–156, Apr. 2018.

[2] G. Zhu, Y. Ma, and S. Hu, "Single-parameter-learning-based finite-time tracking control of underactuated MSVs under input saturation," *Control Eng. Pract.*, vol. 105, Dec. 2020, Art. no. 104652.

[3] G. Shao, Y. Ma, R. Malekian, X. Yan, and Z. Li, "A novel cooperative platform design for coupled USV–UAV systems," *IEEE Trans. Ind. Informat.*, vol. 15, no. 9, pp. 4913–4922, Sep. 2019.

[4] Z. Peng, J. Wang, and D. Wang, "Distributed maneuvering of autonomous surface vehicles based on neurodynamic optimization and fuzzy approximation," *IEEE Trans. Control Syst. Technol.*, vol. 26, no. 3, pp. 1083–1090, May 2018.

[5] L. Hu *et al.*, "A multiobjective optimization approach for COLREGs-compliant path planning of autonomous surface vehicles verified on networked bridge simulators," *IEEE Trans. Intell. Transp. Syst.*, vol. 21, no. 3, pp. 1167–1179, Mar. 2020.

[6] L. Paull, S. Saeedi, M. Seto, and H. Li, "Sensor-driven online coverage planning for autonomous underwater vehicles," *IEEE/ASME Trans. Mechatronics*, vol. 18, no. 6, pp. 1827–1838, Dec. 2012.

[7] L. Huang, M. Zhou, and K. Hao, "Non-dominated immune-endocrine short feedback algorithm for multi-robot maritime patrolling," *IEEE Trans. Intell. Transp. Syst.*, vol. 21, no. 1, pp. 362–373, Feb. 2019.

[8] J. Takahashi, T. Yamaguchi, K. Sekiyama, and T. Fukuda, "Communication timing control and topology reconfiguration of a sink-free meshed sensor network with mobile robots," *IEEE/ASME Trans. Mechatronics*, vol. 14, no. 2, pp. 187–197, Apr. 2009.

[9] B. Irani, J. Wang, and W. Chen, "A localizability constraint-based path planning method for autonomous vehicles," *IEEE Trans. Intell. Transp. Syst.*, vol. 20, no. 7, pp. 2593–2604, Jul. 2019.

[10] G. Han *et al.*, "Ant-colony-based complete-coverage path-planning algorithm for underwater gliders in ocean areas with thermoclines," *IEEE Trans. Veh. Technol.*, vol. 69, no. 8, pp. 8959–8971, Aug. 2020.

[11] M. Mahi, Ö. K. Baykan, and H. Kodaz, "A new hybrid method based on particle swarm optimization, ant colony optimization and 3-opt algorithms for traveling salesman problem," *Appl. Soft Comput.*, vol. 30, pp. 484–490, May 2015.

[12] M. Hassan, A. Hamid, and M. Alkinani, "Ant colony optimization for multi-objective multicast routing," *Comput., Mater. Continua*, vol. 63, no. 3, pp. 1159–1173, 2020.

[13] L. Xie, S. Xue, J. Zhang, M. Zhang, W. Tian, and S. Haugen, "A path planning approach based on multi-direction A* algorithm for ships navigating within wind farm waters," *Ocean Eng.*, vol. 184, pp. 311–322, Jul. 2019.

[14] J. Song and S. Gupta, "ε^*: An online coverage path planning algorithm," *IEEE Trans. Robot.*, vol. 34, no. 2, pp. 526–533, Feb. 2018.

[15] V. An, Z. Qu, F. Crosby, R. Roberts, and V. An, "A triangulation-based coverage path planning," *IEEE Trans. Syst., Man, Cybern. Syst.*, vol. 50, no. 6, pp. 2157–2169, Jun. 2020.

[16] V. An, Z. Qu, and R. Roberts, "A rainbow coverage path planning for a patrolling mobile robot with circular sensing range," *IEEE Trans. Syst., Man, Cybern. Syst.*, vol. 48, no. 8, pp. 1238–1254, Aug. 2018.

[17] M. Hassan and D. Liu, "PPCPP: A predator–prey-based approach to adaptive coverage path planning," *IEEE Trans. Robot.*, vol. 36, no. 1, pp. 284–301, Feb. 2020.

[18] Y. Zuo, R. Tharmarasa, R. Jassemi-Zargani, N. Kashyap, J. Thiyagalingam, and T. T. Kirubarajan, "MILP formulation for aircraft path planning in persistent surveillance," *IEEE Trans. Aerosp. Electron. Syst.*, vol. 56, no. 5, pp. 3796–3811, Oct. 2020.

[19] Z. Peng, J. Wang, and D. Wang, "Distributed containment maneuvering of multiple marine vessels via neurodynamics-based output feedback," *IEEE Trans. Ind. Electron.*, vol. 64, no. 5, pp. 3831–3839, May 2017.

[20] K. Wu, M. A. Esfahani, S. Yuan, and H. Wang, "TDPP-Net: Achieving three-dimensional path planning via a deep neural network architecture," *Neurocomputing*, vol. 357, pp. 151–162, Sep. 2019.

[21] A. Yazici, G. Kirlik, O. Parlaktuna, and A. Sipahioglu, "A dynamic path planning approach for multirobot sensor-based coverage considering energy constraints," *IEEE Trans. Cybern.*, vol. 44, no. 3, pp. 305–314, Mar. 2014.

[22] W. Dong, S. Liu, Y. Ding, X. Sheng, and X. Zhu, "An artificially weighted spanning tree coverage algorithm for decentralized flying robots," *IEEE Trans. Autom. Sci. Eng.*, vol. 17, no. 4, pp. 1689–1698, Oct. 2020.

[23] C. Luo, S. X. Yang, X. Li, and M. Q.-H. Meng, "Neural-dynamics-driven complete area coverage navigation through cooperation of multiple mobile robots," *IEEE Trans. Ind. Electron.*, vol. 64, no. 1, pp. 750–760, Jan. 2016.

[24] Z. Huang, D. Chu, C. Wu, and Y. He, "Path planning and cooperative control for automated vehicle platoon using hybrid automata," *IEEE Trans. Intell. Transp. Syst.*, vol. 20, no. 3, pp. 959–974, Mar. 2019.

[25] J. Vilca, L. Adouane, and Y. Mezouar, "Stable and flexible multi-vehicle navigation based on dynamic inter-target distance matrix," *IEEE Trans. Intell. Transp. Syst.*, vol. 20, no. 4, pp. 1416–1431, Apr. 2019.

[26] F. Fabiani and S. Grammatico, "Multi-vehicle automated driving as a generalized mixed-integer potential game," *IEEE Trans. Intell. Transp. Syst.*, vol. 21, no. 3, pp. 1064–1073, Mar. 2020.

[27] T. Yang, J. V. Miro, Q. Lai, Y. Wang, and R. Xiong, "Cellular decomposition for nonrepetitive coverage task with minimum discontinuities," *IEEE/ASME Trans. Mechatronics*, vol. 25, no. 4, pp. 1698–1708, Aug. 2020.

[28] H. Wang, Z. Li, Y. Li, B. B. Gupta, and C. Choi, "Visual saliency guided complex image retrieval," *Pattern Recognit. Lett.*, vol. 130, pp. 64–72, Feb. 2020.

[29] H. Fatemidokht, M. K. Rafsanjani, B. B. Gupta, and C.-H. Hsu, "Efficient and secure routing protocol based on artificial intelligence algorithms with UAV-assisted for vehicular ad hoc networks in intelligent transportation systems," *IEEE Trans. Intell. Transp. Syst.*, vol. 22, no. 7, pp. 4757–4769, Jul. 2021.

Yong Ma (Member, IEEE) received the B.Sc. degree from the Wuhan University of Technology (WUT) in 2006, the M.Sc. degree from Dalian Maritime University in 2008, and the Ph.D. degree from the Huazhong University of Science and Technology, China, in 2012. He is currently a Full Professor with the Department of Maritime Management, School of Navigation, WUT. His current research interests include intelligent algorithms for unmanned vehicles, navigation, and control.

Yujiao Zhao is currently pursuing the Ph.D. degree with the School of Navigation, Wuhan University of Technology. His current research interests include the path following of unmanned surface vehicle and deep reinforcement learning.

Zhixiong Li (Senior Member, IEEE) received the Ph.D. degree in transportation engineering from the Wuhan the University of Technology, China, in 2013. He is currently with the Faculty of Mechanical Engineering, Opole University of Technology, and also with the Yonsi Frontier Laboratory, Yonsei University. His research interests include intelligent vehicles and control, loop closure detection, and mechanical system modeling and control.

Huaxiong Bi received the M.Sc. degree from the School of Navigation, Wuhan University of Technology, in 2020. His current research interest includes the coverage path planning of unmanned surface vehicle.

Jing Wang is currently pursuing the M.Sc. degree with the School of Navigation, Wuhan University of Technology. His current research interest includes the coverage path planning of unmanned surface vehicle.

Reza Malekian (Senior Member, IEEE) is currently with the Department of Computer Science and Media Technology, Malmö University, Malmö, Sweden. His current research interests include the Internet of Things and sensors in intelligent transportation systems. He is also a Co-Founder of the IEEE Vehicular Technology Society (VTS) South Africa Chapter and a member of the IEEE Signal Processing Society Chapters Committee.

Miguel Angel Sotelo (Fellow, IEEE) received the Ph.D. degree in electrical engineering from the University of Alcalá (UAH), Madrid, Spain, in 2001. He is currently a Full Professor with the Department of Computer Engineering, UAH. His research interests include autonomous vehicles and prediction of intentions.